Molecular Dynamics Analysis of Interfacial Structures and Sum Frequency Generation Spectra of Aqueous Hydrogen Halide Solutions†

Tatsuya Ishiyama‡ and Akihiro Morita*,‡,§

Department of Chemistry, Graduate School of Science, Tohoku University, Sendai 980-8578, Japan and Department of Computational Molecular Science, Institute for Molecular Science, Okazaki 444-8585, Japan

Received: April 18, 2007; In Final Form: June 27, 2007

Molecular dynamics simulation for gas/liquid interfaces of aqueous hydrochloric (HCl) and hydroiodic (HI) acid solutions is performed to calculate and analyze their sum frequency generation (SFG) spectra. The present MD simulation supports the strong preference of hydronium ions at the topmost surface layer and a consequent formation of ionic double layers by the hydronium and halide ions near the interface. Accordingly, the orientational order of surface water in the double layers is reversed in the acid solutions from that in the salt (NaCl or NaI). The calculated SFG spectra of the O−H stretching region reproduce the experimental spectra of ssp and sps polarizations well. In the ssp spectra, the strong enhancement in the hydrogen-bonding region for the acid solutions is elucidated by two mechanisms, ordered orientation of water in the double layer and symmetric OH stretching of the surface hydronium ions. In the sps spectra, reversed orientation of surface water is evidenced in the spectral line shapes, which are quite different from those of the salt solutions.

1. Introduction

Understanding of vapor/liquid aqueous interfaces has been greatly elaborated for the past decade both theoretically[1] and experimentally.[2] The conventional image charge model[3] predicts that ions are repelled from the aqueous electrolyte interfaces, whereas recent molecular dynamics (MD) simulation argued that ions are not necessarily repelled from the interface and that the chemical character of ions makes significant differences in the interfacial structure at a molecular level. The structure of the aqueous interfaces is also pertinent to heterogeneous atmospheric chemistry,[1,2,4,5] where the surface concentration of ions could be an important factor to determine the kinetics of surface-specific reactions. Such recent interests in aqueous interfaces have prompted further investigation of liquid interfaces via surface-specific experimental means. While available experimental probes of liquid interfaces are quite limited, second-order nonlinear spectroscopy,[6,7] including second harmonic generation or sum frequency generation, is quite appropriate to study liquid interfaces at a molecular level.[8−13] In particular, sum frequency generation (SFG) spectroscopy is a versatile experimental probe of interfacial vibrational spectra, and hence, a number of aqueous interfacial structures have been investigated by this nonlinear optical method.[2,14]

The SFG experiment, however, often suffers from ambiguities in interpretation of the observed spectra, partly because spectral decomposition of overlapping bands is often not unique.[15] This situation is particularly serious in the O−H stretching region of aqueous interfaces, where extensive overlap of various red-shifted components complicates its spectral assignment. Thus, a close collaboration with advanced theoretical analysis is helpful for an accurate interpretation of the spectra.[16−20] In fact, the MD analysis can offer more insight into SFG spectroscopy beyond the decomposition of overlapping bands to sophisticate our understandings on interfacial structure. For example, our previous studies of aqueous salt (NaCl and NaI) solutions[21−23] revealed that the SFG intensity is strongly influenced by the intermolecular vibrational correlation, which distorts the commonly accepted relationship between the susceptibility and molecular orientation. The MD analysis also argued that the SFG spectra of different polarization combinations shed light on the ionic double-layer formation in a quite distinct manner. In particular, the sps spectra of the aqueous solutions are found to sensitively reflect the double-layer structure, though microscopic interpretation of sps spectra is considered less intuitive than that of ssp. (The notation ssp or sps designates the polarization combination of SFG, visible, and infrared lights, respectively, where p denotes the polarization parallel to the incident plane and s the polarization perpendicular to it.) These findings demonstrate a need of more refined analysis of SFG spectra of aqueous interfaces beyond the empirical decomposition analysis. In the present study, we address aqueous acid (HCl and HI) solution interfaces, where hydronium ions could play a characteristic role at the interfaces, as discussed in the followings.

It has been recognized for a long time that surface tension and surface potential measurements have implied a distinct behavior of the acid solution surfaces from that of other salt solutions. Randles reported a general tendency from a comprehensive measurement of those quantities[24] that addition of most inorganic salts into water raises the surface tension, indicating a negative surface excess of ions, whereas most acids show less tendency or even the opposite trend, from which it is suggested that the hydronium ion is more surface active than other alkali cations. Surface potential measurements, on the other hand, reported that addition of the acids gives a larger positive perturbation on the surface potential than other salt solutions, which appears puzzling since hydronium is suggested to be more surface active than other cations.[24] We should note that such

† Part of the "Sheng Hsien Lin Festschrift".

* To whom correspondence should be addressed. E-mail: amorita@mail.tains.tohoku.ac.jp.

‡Tohoku University.

§Institute for Molecular Science.

10.1021/jp072997z CCC: $37.00
Published on Web 08/18/2007

thermodynamic measurements do not yield direct structural information at a monolayer level, and further investigation is called for.

Regarding the location of hydronium ions near the interface, recent MD simulations of acid solution surfaces show some quantitative discrepancies. Dang reported no definite minimum in the calculated free-energy profile of the hydronium ion at the surface region,[25] whereas a classical MD simulation by Mucha et al.[26] and a simulation using the multistate empirical valence bond model by Voth and co-workers[27] predicted enriched hydronium ions near the surface region. These results indicate that the concentration profile of the hydronium ions is sensitive to the molecular model employed, and thus, the MD results should be verified by some reliable experiments with sufficient surface sensitivity. We also note in passing that the preferential location of a hydronium ion at the surface has been implied in fairly large protonated water clusters $H^+(H_2O)_n$ ($n \sim 21$)[28] via vibrational spectroscopy and ab initio calculation, though no conclusive evidence is available yet.

A pioneering work of the SFG study for HCl solution was performed by Baldelli et al.,[29] in which some characteristic features of the ssp-polarized spectra were reported. One of the most striking features in the ssp-polarized SFG spectra is seen in the intensity at the $\sim$3200 cm^{-1} region, usually assigned as the "ice-like band", as a function of HCl concentration. With increasing concentration up to about $0.03x$ (x = mole fraction), the SFG intensity at this region is strongly enhanced, whereas more acidification decreases the intensity. This turnover feature for the HCl solution has been also reported in the other experimental studies[26,30] and for HI and other acid solutions.[26,31,32] The interpretation for the enhancement in the lower concentration range is, however, somewhat controversial[2] and remains unsolved. Baldelli et al. elucidated this enhancement from the perturbed orientational structure of solvent water molecules, which is caused by the electric double layer between the hydronium cation and chloride anion.[29] Allen and co-workers, on the other hand, attributed the augmented intensity to a vibrational SFG response from hydronium cations.[26,33]

In this Article, we present an intensive MD analysis of the SFG spectra of the aqueous acid solutions, particularly in comparison with those of salt solutions. Our focus will include (i) the origin of enhancement at the 3200 cm^{-1} region mentioned above and (ii) whether the observed SFG spectra consistently indicate surface solvation of hydronium ions or the ionic double-layer structure of the acid solutions. The remainder of this paper is organized as follows. Section 2 describes the MD simulation methodology, including molecular models, computation, and analysis of SFG spectra. Section 3 discusses the interfacial structures such as density profiles and the orientational order of molecules. In section 4, the calculated SFG spectra of two polarization combinations, ssp and sps, and their susceptibility including the phase information are analyzed. Section 5 is devoted to conclusions.

2. Simulation Method

2.1. Molecular Models and Conditions. Aqueous 1.1 M HCl and HI solutions are assumed to consist of hydronium cations H_3O^+, halide anions Cl^- or I^-, and the solvent H_2O molecules. These constituent molecules are treated by flexible and polarizable classical models. Flexibility (internal vibration) in the models of H_2O and H_3O^+ is necessary for evaluating vibrational SFG spectra using the time correlation formalism,[17] and the electronic polarization effect is essential for an accurate description of ions at the interface.[1,34] In the classical models, the acid is considered to be fully ionized, which is a reasonable assumption for the strong acids at this concentration. Though the classical model of the hydronium cation does not explicitly allow for proton transfer or the Zundel form, equilibrium structural properties of the aqueous interfaces are reasonably represented with classical models.[26]

The potential energy of the whole system using the flexible and polarizable models is written as

$$U_{\text{total}} = U_{\text{intra}} + U_{\text{pair}} + U_{\text{pol}} \tag{1}$$

where U_{intra} refers to the intramolecular vibrational potential for H_2O and H_3O^+, U_{pair} to the intermolecular site−site pairwise interaction of van der Waals and Coulomb terms, and U_{pol} to the nonadditive induced polarization. In the present study, the electronic polarization is modeled with a point dipole polarizability located at each molecule. For H_2O, we use the flexible and polarizable model that we have previously developed for describing aqueous interfaces and SFG spectra.[22] For Cl^- and I^-, a point dipole model[35] is employed, which was also used in our previous study.[22] For H_3O^+, we have employed an intramolecular force field given by Tuckerman and co-workers[36,37] using a Morse potential for OH stretching and a harmonic potential for bending

$$u_{\text{intra}}^{H_3O^+} = \sum_{k=1}^{3} D_{\text{h}}(1 - \exp[-\alpha_{\text{h}}(r_k - r_{\text{h,eq}})])^2 + \sum_{k=1}^{3} \frac{K_{\text{h}}}{2}(\theta_k - \theta_{\text{h,eq}})^2 \tag{2}$$

where r_k and θ_k are respectively the kth OH bond length and HOH angle. The values of parameters D_{h}, α_{h}, $r_{\text{h,eq}}$, K_{h}, and $\theta_{\text{h,eq}}$ are listed in the original papers.[36,37] The intermolecular interaction of H_3O^+ is represented by the parameters of Lennard-Jones, Coulombic, and a point polarizability, which were given by Dang.[25]

Other conditions of MD simulation are same as those of our previous study on salt solutions[22] and thus briefly summarized in the following. The MD simulations are executed using a slab geometry of liquid in a rectangular simulation cell with dimensions of $L_x \times L_y \times L_z = 30$ Å $\times$ 30 Å $\times$ 150 Å, where the z axis is normal to the vapor/liquid interfaces, and the Ewald summation is used for treating long-range interactions. The simulation cell contains 1000 (water) + 20 (hydronium cation) + 20 (halide anion) molecules, which corresponds to a 1.1 M aqueous solution system. Constant-energy MD simulation is executed after equilibrating the system for 100 ps at 298 K. The statistics were taken for a total of 30 ns with parallel computations. The computation was performed on the Hitachi HA8000 machine at the Research Center of Computational Science in Okazaki, Japan.

2.2. Calculation of SFG Spectra. For the analysis of SFG spectroscopy, information on the frequency-dependent, second-order nonlinear susceptibility χ for the interface is crucial. The methodology to calculate χ by MD simulation has been proposed in two ways, that is, the one based on the energy representation of χ[16] and the one based on the time correlation function (TCF) representation.[17,18] While the two representations are formally equivalent, the latter is more suitable for nonempirical computation of SFG spectra, partly because it is capable of readily incorporating the motional effect[38] and the intermolecular vibrational correlation effect.[21] Thus, the present work employs the TCF method for computation. Since the computational

details were described elsewhere,[23] here, we briefly summarize the procedure below.

The SFG intensity line shape I^{SFG} is given as proportional to the square of the frequency-dependent second-order nonlinear susceptibility, $|\chi(\omega_{SFG}, \omega_{vis}, \omega_{IR})|^2$, where ω_{vis} and ω_{IR} are the frequencies of the input visible and infrared fields, respectively, and $\omega_{SFG} = \omega_{vis} + \omega_{IR}$ is the output sum frequency. Here, we note that the dispersion in the local field at the frequency ω_{IR} is incorporated in the present definition of χ. Regarding the polarization combinations, the intensity line shape of the ssp and sps polarizations is calculated via[10,14]

$$I_{ssp}^{SFG} \propto |\chi_{iiz}|^2 \quad I_{sps}^{SFG} \propto |\chi_{izi}|^2 \tag{3}$$

where the subscript z denotes the laboratory-fixed coordinate normal to the gas−liquid interface and i stands for the lateral coordinate, either x or y. The nonlinear susceptibility χ is composed of the vibrationally resonant part χ^R and the nonresonant part χ^{NR}, that is, $\chi = \chi^R + \chi^{NR}$. χ^R is classically represented with the time correlation function between the dipole moment $\boldsymbol{M}$ and the polarizability tensor $\boldsymbol{A}$ of the system with an appropriate quantum correction[18]

$$\chi_{pqr}^R = \frac{i\omega_{IR}}{2k_BT}\int_0^\infty dt\, e^{i\omega_{IR}t}\langle A_{pq}(t)M_r(0)\rangle_{cl} \tag{4}$$

where k_B and T are respectively the Boltzmann constant and temperature, and $\langle\rangle_{cl}$ indicates the statistical average in the classical mechanics. χ^{NR} is empirically determined as independent of ω_{IR} so as to best describe the experimental SFG spectra.

In eq 4, the instantaneous dipole and polarizability of the whole system at time t, $\boldsymbol{M}(t)$ and $\boldsymbol{A}(t)$, are given with those of constituent molecules as

$$\boldsymbol{M}(t) = \sum_i \boldsymbol{p}_i(t) \quad \boldsymbol{A}(t) = \sum_i \boldsymbol{\alpha}_i^{eff}(t) \tag{5}$$

where $\boldsymbol{p}_i(t)$ is the dipole moment of the ith molecule at time t and $\boldsymbol{\alpha}_i^{eff}(t)$ is the effective polarizability tensor of the ith molecule including the local field correction.[17] During the time development of the MD trajectory, $\boldsymbol{p}_i(t)$ and $\boldsymbol{\alpha}_i^{eff}$ are calculated at each time step t by taking account of the intermolecular electrostatic interactions at the instantaneous configuration.

In the actual MD calculations, we applied a "filtering function"[23] to eq 5 in order to cut off the noise from the bulk region deeper than the $\hat{z}_r$ plane with $\hat{z}_r = -10$ Å.

2.3. Decomposition Analyses of χ. The time correlation representation of χ^R in eq 4 allows for further investigation of SFG spectroscopy through decomposition analyses of χ^R. We present two decomposition schemes in the followings. The first scheme is to decompose χ^R into the so-called self-part χ^R(self) and the correlation part χ^R(corr)[21,23]

$$\chi_{pqr}^R = \chi_{pqr}^R(\text{self}) + \chi_{pqr}^R(\text{corr}) \tag{6a}$$

$$\chi_{pqr}^R(\text{self}) = \frac{i\omega_{IR}}{2k_BT}\sum_i \int_0^\infty dt\, e^{i\omega_{IR}t}\langle \alpha_{i,pq}^{eff}(t)p_{i,r}(0)\rangle \tag{6b}$$

$$\chi_{pqr}^R(\text{corr}) = \frac{i\omega_{IR}}{2k_BT}\sum_i \sum_{j(\neq i)} \int_0^\infty dt\, e^{i\omega_{IR}t}\langle \alpha_{i,pq}^{eff}(t)p_{j,r}(0)\rangle \tag{6c}$$

where χ^R(self) consists of the intramolecular correlation of $\boldsymbol{\alpha}_i^{eff}$ and $\boldsymbol{p}_i$ and χ_{pqr}^R(corr) consists of the intermolecular correlation ($i \neq j$). Note that χ^R(self) is naturally represented as the sum of molecular contributions $\chi^R(\text{self}) = \sum_i^N \beta_i^{eff}$ and consequently interpreted as the product of the number density N and the average molecular hyperpolarizability $\langle\beta\rangle$, $N\langle\beta\rangle$. However, in a system consisting of strongly interacting molecules, such as aqueous salt solutions, we have previously demonstrated that χ^R(corr) significantly contributes to χ^R, which breaks the intuitive assumption that χ is simply given by N and $\langle\beta\rangle$.[21,23]

The second scheme is to decompose χ^R into contributions of species. In the case of an aqueous electrolyte solution, the decomposition of χ^R can be performed into water (W) and ions (I) as[21,23]

$$\chi_{pqr}^R = \chi_{pqr}^{R,WW} + \chi_{pqr}^{R,WI} + \chi_{pqr}^{R,IW} + \chi_{pqr}^{R,II} \tag{7a}$$

$$\chi_{pqr}^{R,mn} = \frac{i\omega_{IR}}{2k_BT}\int_0^\infty dt\, e^{i\omega_{IR}t}\langle A_{pq}^m(0)M_r^n(t)\rangle \tag{7b}$$

A_{pq}^m and M_r^m (m = W or I) in eq 7 respectively denote the sum of the effective polarizability and the dipole of species m

$$A_{pq}^m(t) = \sum_i^{\text{species m}} \alpha_{i,pq}^{eff}(t) \quad M_r^m(t) = \sum_i^{\text{species m}} p_{i,r}(t) \tag{8}$$

where the summation of i is restricted to the species m. In eq 7, $\chi^{R,WW}$ and $\chi^{R,II}$ are attributed to the contribution of water and ions, respectively, and $\chi^{R,WI}$ and $\chi^{R,IW}$ to the cross correlation of water and ions. We will utilized these above decomposition schemes for SFG analysis in section 4.

3. Interfacial Structures

3.1. Surface Density Profiles. Figure 1 shows the calculated density profiles of constituent species near the gas−liquid interfaces of 1.1 M HCl and HI aqueous solutions, where the density of species is defined at the center-of-mass location of molecules. The ordinate is normalized with the bulk density of each component, and the abscissa is plotted using the local z coordinate, $\hat{z}$, with the origin being located at the Gibbs dividing surface of solvent water. Hereafter, this local coordinate $\hat{z}$ will be employed, where $\hat{z} > 0$ designates the vapor side and $\hat{z} < 0$ the liquid side of the Gibbs dividing surface.

In the HCl case (panel a), an enhanced H_3O^+ concentration of $\rho/\rho_{bulk} \sim 1.55$ is observed at $\hat{z} \sim -0.5$Å, which is qualitatively consistent with the recent theoretical studies.[25−27] The density of Cl^- also has a peak of $\rho/\rho_{bulk} \sim 1.4$ at $\hat{z} \sim -5$Å. The deviation in the peak positions of H_3O^+ and Cl^- indicates an electric double-layer formation with a separation width of about 4.5 Å. We note that the double-layer structure is less obvious in a previous MD calculation of HCl solution using a rigid-polarizable model,[26] implying that the interface structure somewhat depends on the molecular model of species. The local structure of interfaces should be examined through critical comparison of MD results and SFG experiments with varying polarizations, as presented in the next section.

In the case of the HI solution (panel b), an analogous electric double layer between H_3O^+ and I^- is seen, while the separation width of the ionic double layers decreases and the peak concentrations of ions are enhanced. The maximum concentrations of ions are calculated to be $\rho/\rho_{bulk} \sim 2.3$ at $\hat{z} \sim -0.5$Å for H_3O^+ and $\rho/\rho_{bulk} \sim 2.2$ at $\hat{z} \sim -2$Å for I^-, resulting in a separation width of 1.5 Å. Comparing the panel b with a, one finds that the location of the H_3O^+ layer changes little, whereas the peak of the I^- layer comes closes to the interface than the Cl^- layer. This different character of anions is consistent with

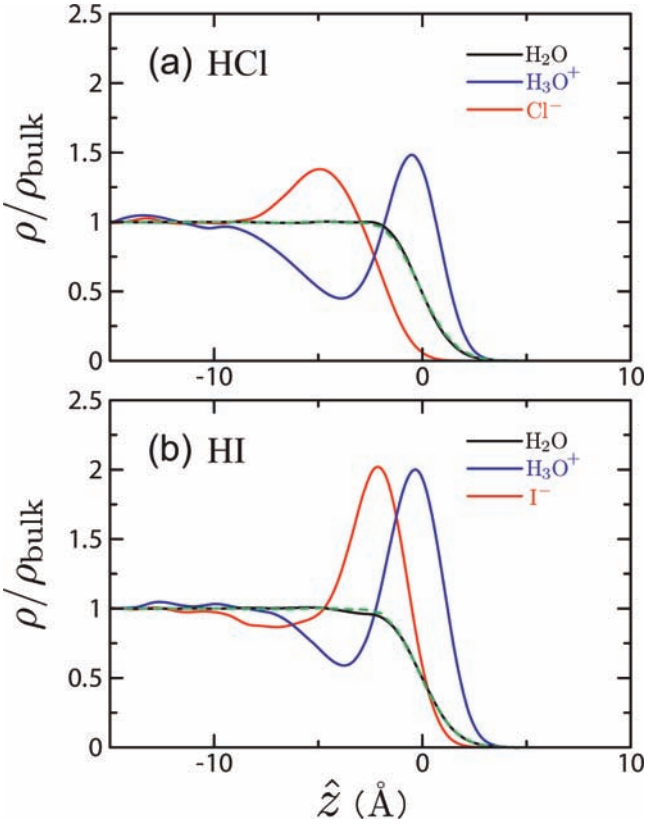

Figure 1. Normalized density profile of each species near the gas−liquid interfaces of 1.1 M HCl (panel a) and HI (panel b) solutions. In both panels, the density profile of pure water is shown with the green dashed lines for comparison.

the fact that iodide is more surface active than chloride. Consequently, the smaller separation of the H_3O^+ and I^- layers should stabilize the enhanced concentrations in the ion layers.

Comparing Figure 1 for the acid solutions with the density profiles for salt (NaCl or NaI) solutions,[22] we notice that the direction of the electric field in the double layer of the acid solutions is reversed to those of the salt solutions. This is arguably due to the strong surface preference of the hydronium cation. This difference has significant implications in the orientational structure, as discussed below. In a comparison of the 1.1 M HCl solution with the 1.1 M NaI solution, the peak values of the I^- concentration in the HI solution surface are more enhanced than that in the NaI solution ($\rho/\rho_{bulk} \sim 1.75$ for 1.1 M NaI[22]). This result is qualitatively consistent with the SHG experiment by Petersen and Saykally[39] and the MD simulation by Mucha et al.[26]

3.2. Orientational Order of Molecules. Our previous study on the NaI solution surface[22] has demonstrated that the ionic double layer of NaI significantly distorts the orientational order of solvent water. In this subsection, we investigate the orientational structure of water and hydronium in the vicinity of the HCl and HI solution surfaces. To describe the orientation of molecules, we introduce an angle θ between the surface normal and the permanent dipole vector of water or hydronium. The definition is depicted in the insets of Figures 2 and 3 for water and hydronium, respectively, where the permanent dipole vector is given as the sum of two or three constituent OH vectors, that is, $\vec{OH}_1 + \vec{OH}_2$ for water and $\vec{OH}_1 + \vec{OH}_2 + \vec{OH}_3$ for hydronium. Note that this definition of dipole orientation does not include the electronic polarization. The $\cos\theta > 0$ corresponds to the permanent dipole pointing toward the vapor phase, while $\cos\theta < 0$ corresponds to that toward the liquid phase.

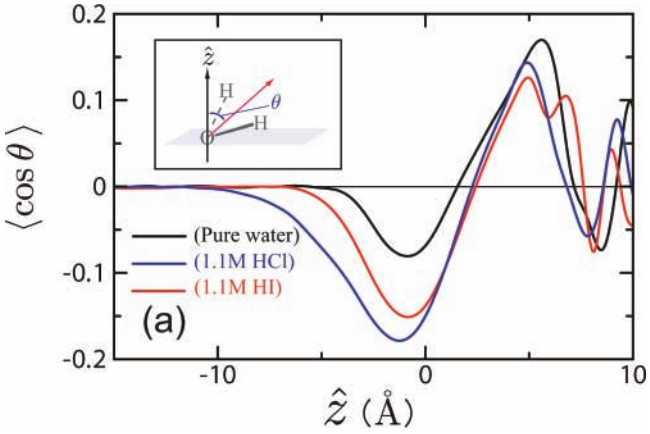

Figure 2. Orientational profiles $\langle\cos\theta(\hat{z})\rangle$ of water for pure water (black) and 1.1 M HCl (blue) and HI (red) aqueous solutions as a function of the depth $\hat{z}$. The θ defines the orientation of the water dipole as illustrated in the inset.

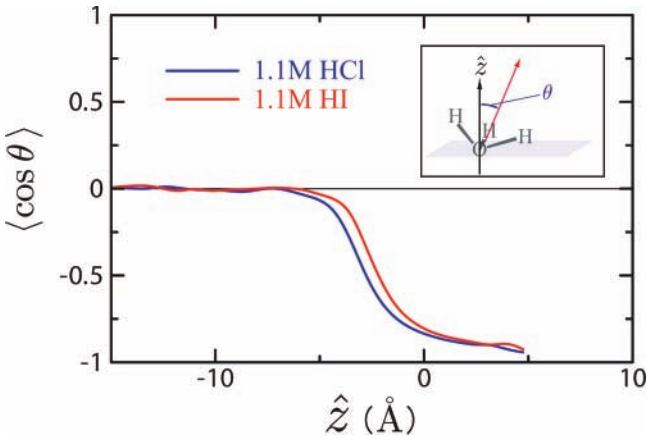

Figure 3. Orientational profiles $\langle\cos\theta(\hat{z})\rangle$ of the hydronium cation for 1.1 M HCl (blue) and HI (red) aqueous solutions. The definition of θ is illustrated in the inset.

Figure 2 shows the average $\langle\cos\theta\rangle$ for water molecules as a function of the depth $\hat{z}$. Comparing the case of pure water (black)[22] with those of the 1.1 M HCl (blue) and 1.1 M HI (red) aqueous solutions, one notices that the large negative dip of $\langle\cos\theta\rangle$ at around the Gibbs dividing surface ($\hat{z} = -5 \sim 2$ Å) is augmented in the acid solutions, which means the water molecules of the acid solutions direct their dipoles toward the liquid phase more strongly than those of pure water. This is obviously due to the electric field generated by the ionic double layer of the hydronium and halide, as illustrated in Figure 1. Figure 2 also shows that the negative dip is more emphasized in the HCl solution than that in HI, indicating that the HCl double layer exerts larger perturbation on the orientational order than HI. Comparing the acid (HCl and HI) solution surfaces with the salt (NaCl and NaI) solutions,[22] we notice that $\langle\cos\theta\rangle$ is negatively perturbed in the acid solution surfaces, whereas it is positively perturbed in the case of the sodium halide (e.g., NaI) solution. This opposite trend is understood from the reverse direction of the electric field within the ionic double layer. These orientational features are reflected in the SFG spectra, as discussed later in detail.

Next, we focus on the orientational structure of hydronium ions for 1.1 M HCl and HI solutions in Figure 3. In the bulk region, apart from the Gibbs dividing surface, hydronium ions of the HCl or HI solution are randomly oriented, resulting in $\langle\cos\theta\rangle \sim 0$, whereas $\langle\cos\theta\rangle$ starts to deviate negatively from zero as it approaches the interfacial region. The negative order

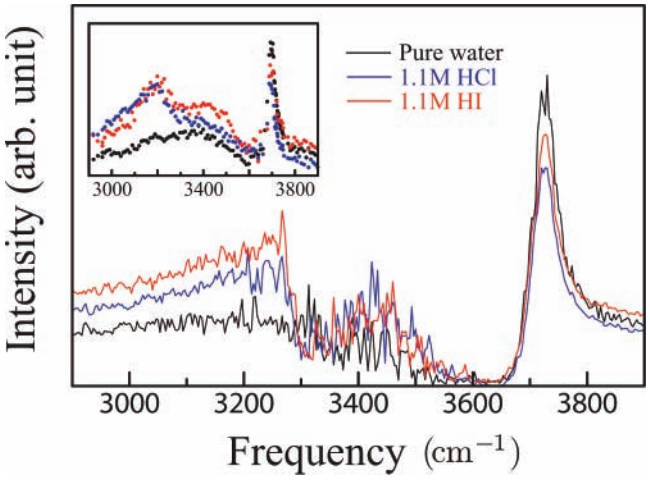

Figure 4. Calculated SFG spectra of ssp polarization for a 1.1 M HCl (blue) solution, 1.1 M HI (red), and pure water (black). The inset shows the experimental SFG spectra of the corresponding 1.2 M solutions and pure water by Mucha et al.[26]

of $\langle \cos \theta \rangle$ indicates that hydronium ions tend to direct their protons (hydrogens) toward the liquid phase.[26,27] Near the Gibbs dividing surface at $\hat{z} \sim 0$, the value of $\langle \cos \theta \rangle$ becomes close to -1, which manifests that the orientation of a hydronium ion there is strongly ordered with its dipole antiparallel to the surface normal. This strong orientational order is understood from the "amphiphilic" nature of the hydronium ion, with the hydrophilic character of its hydrogens and the hydrophobic character of its oxygen. Since the oxygen site carries a weaker minus charge than that of water and accordingly becomes a poor hydrogen bond acceptor, it tends to be located in the vapor side of the surface.[26] Figure 3 shows a small difference in the $\langle \cos \theta \rangle$ profiles for 1.1 M HCl and 1.1 M HI solutions, suggesting a minor role of the counteranions on the orientational order of hydronium ions.

4. Sum Frequency Generation Spectra

4.1. The ssp-Polarized Spectra. Figure 4 shows the calculated ssp-polarized SFG spectra of pure water (black), HCl (blue), and HI (red) solutions, which are compared to the experimental results by Mucha et al.[26] in the inset. We can see that the calculated spectra capture several features of the experimental spectra of the acid solutions well, including (i) relatively strong enhancement in intensity at about 3200 cm^{-1}, (ii) modest enhancement at about 3400 cm^{-1}, and (iii) decreased intensity at the 3700 cm^{-1} peak. In this subsection, we elucidate the origin of these spectral features compared to the spectrum of pure water. We first discuss the feature (iii) in the following, and the analysis of (i) and (ii) follows, with the help of the decomposition of χ described in section 2.3.

The band at about 3700 cm^{-1} is assigned to the dangling (free) OH of water.[40] The present calculation reproduces the order of its peak intensity observed experimentally,[26] (pure water) > (HI) > (HCl). The reduced intensity for the acids was interpreted as a consequence of the diminishing surface density of the free OH bonds of water.[26] This interpretation is also consistent with our calculated orientational structure in Figure 2, where the positive region of $\langle \cos \theta \rangle$ at the vapor side of the Gibbs dividing surface ($0 \lesssim \hat{z} \lesssim 5$ Å) is diminished more for the HCl or HI solution than for pure water, implying that a considerable part of the OH bonds should be reoriented to the liquid side at the vapor side of the Gibbs dividing surface. Larger perturbation of HCl than of HI on the surface structure, which is implicated in section 3, is also reflected in the peak intensity at about 3700 cm^{-1} in Figure 4.

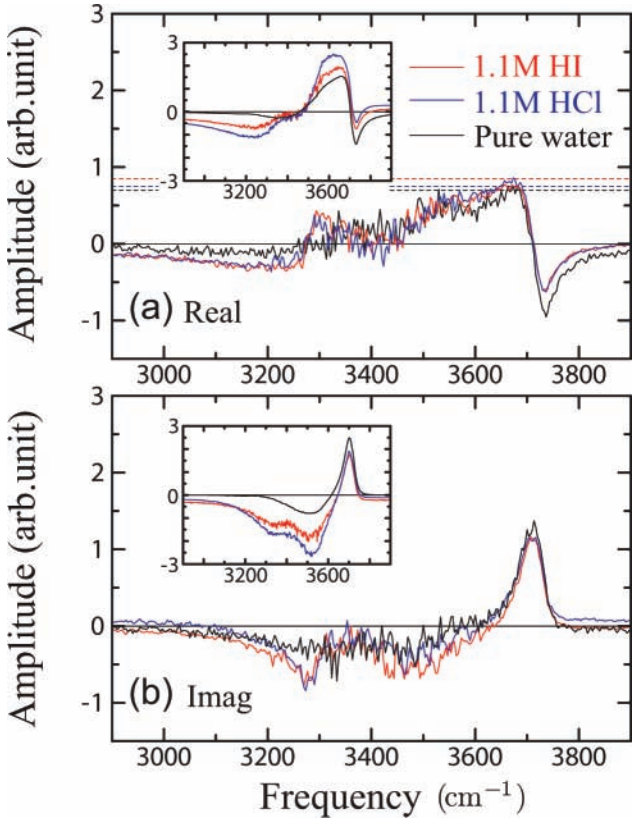

Figure 5. (a) Real and (b) imaginary parts of the iiz ($i = x, y$) nonlinear susceptibility, χ^{R}_{iiz}, for HCl and HI solutions and pure water. The insets show the self-part, χ^{R}_{iiz}(self). The dashed horizontal lines in panel a indicate $-\chi^{NR}_{iiz}$.

Nonlinear Susceptibility χ^{R}_{izz}. The computational SFG analysis by MD simulation has a practical advantage of obtaining the nonlinear susceptibility, a complex quantity involving both amplitude and phase, whereas ordinary SFG experiments can detect only the amplitude in eq 3. The phase of χ^{R} provides us with an informative relation between SFG spectra and surface structures, though the phase information has not been fully explored yet by experiments.[41] In particular, the sign of the imaginary part, Im[χ^{R}_{iiz}], reflects the orientation of transition dipoles with respect to the surface normal.[21]

Figure 5 shows the real (panel a) and imaginary (panel b) parts of χ^{R}_{iiz} for HCl (blue) and HI (red) solutions, where those of pure water are also displayed with black lines for comparison. We notice the band at about 3280 cm^{-1} is conspicuously enhanced in Im[χ^{R}_{iiz}] for hydrogen halide solutions. This band contributes to the relatively strong enhancement of the SFG spectra at this frequency region in Figure 4.

Figure 5 also shows the self-part χ^{R}(self), which is discussed in section 2.3, in the insets. In a comparison of χ^{R} with χ^{R}(self), the amplitude of χ^{R}(self) is larger than that of χ^{R} throughout the spectral region from 3000 to 3700 cm^{-1}. The mechanism of the reduced amplitude of χ^{R} in the ssp-polarized case has been elucidated by the intermolecular correlation effect.[21,23]

Contribution of Species in χ^{R}_{izz}. Next, we apply the second decomposition scheme of χ^{R}_{iiz} into the contribution from each species, as discussed in section 2.3, to elucidate the perturbations in the hydrogen-bonding region.

Figure 6 shows the decomposition results based on eq 7 of the imaginary part of χ^{R}_{iiz}, where Im[χ^{R}_{iiz}] in Figure 5 is

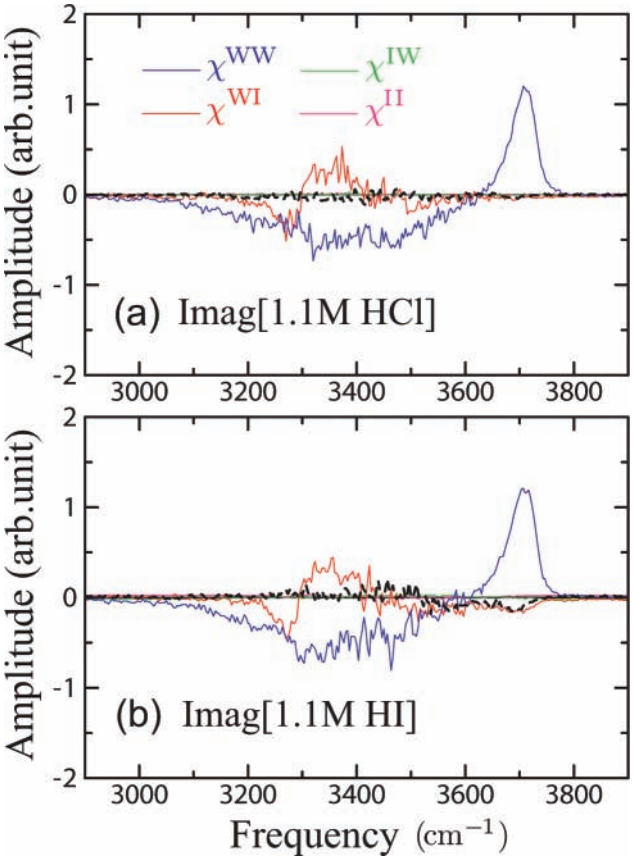

Figure 6. Decomposed amplitudes of Im[χ^{R}_{iiz}] from eq 7 for HCl (panel a) and HI (panel b) solutions. The black dotted line indicates Im[$\chi^{WI,ind}$] defined by eq 9c.

decomposed into Im[χ^{R}_{iiz}] = Im[$\chi^{R,WW}_{iiz}$] + Im[$\chi^{R,WI}_{iiz}$] + Im[$\chi^{R,IW}_{iiz}$] + Im[$\chi^{R,II}_{iiz}$]. It is obvious in Figure 6 that $\chi^{R,IW}_{iiz}$ (green lines) and $\chi^{R,II}_{iiz}$ (pink lines) are much weaker than $\chi^{R,WW}_{iiz}$ (blue lines) and $\chi^{R,WI}_{iiz}$ (red lines), and consequently, the total χ^{R}_{iiz} is governed by the latter two components. The former two minor components are associated with the polarizabilities of ions, which have essentially no vibrational component in the water OH stretching region.[21] The two major components, $\chi^{R,WW}_{iiz}$ and $\chi^{R,WI}_{iiz}$, have quite different spectral line shapes from each other in Figure 6. The water−water component, Im[$\chi^{R,WW}_{iiz}$] (blue lines), shows considerable negative amplitude over the hydrogen-bonding region, 3000−3600 cm^{-1}. This is attributed to the orientation of surface water molecules, which direct their dipoles toward the liquid phase strongly due to the electric double layer, as indicated in Figure 2. This component contributes to the enhanced intensity in the SFG spectra of the acid solutions in the hydrogen-bonding region at about 3200 and 3400 cm^{-1} (see Figure 4).

On the other hand, the water−ion correlation term, $\chi^{R,WI}_{iiz}$ (red lines), changes its imaginary sign within 3200−3400 cm^{-1}, which is negative at the lower frequency and positive at the higher frequency region. The negative component of Im[$\chi^{R,WI}_{iiz}$] augments the SFG intensity at about 3280 cm^{-1} in Figure 4, while the positive component contributes to the intensity dip at about 3300−3350 cm^{-1} in Figure 4. In the following, we discuss the mechanism of water−ion correlation, which manifests in the $\chi^{R,WI}_{iiz}$ term, and elucidate that (I) the contribution of ions in $\chi^{R,WI}_{iiz}$ in the hydrogen-bonding region actually comes from intramolecular vibration of hydronium cations and (II) the reverse sign of Im[$\chi^{R,WI}_{iiz}$] in 3200−3400 cm^{-1} originates from

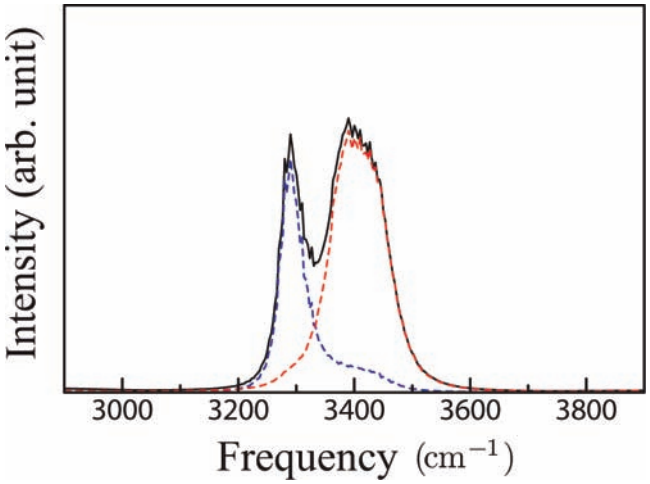

Figure 7. Vibrational density of state for hydronium ions at the topmost layer of a 1.1 M HCl solution. The black solid line indicates the total $I^{vdos}(\omega)$ in eq 11, whereas the blue dashed line and red dashed line indicate the symmetric stretching component, $I^{vdos}_{1,1}(\omega)$, and degenerate stretching components, $I^{vdos}_{2,2}(\omega)$ + $I^{vdos}_{3,3}(\omega)$, respectively (see Appendix).

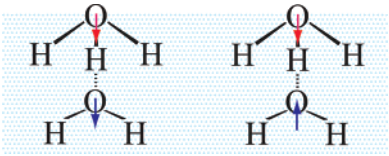

Figure 8. Two schematic pictures of the dipole correlation between a hydronium ion at the surface and a hydrogen-bonded neighboring water. The transition dipoles of the hydronium ion and water are illustrated with red and blue arrows, respectively.

the coupling mechanism between water and the symmetric OH stretching mode of the hydronium ion.

Water−Hydronium Coupling in $\chi^{R,WI}_{iiz}$. To demonstrate (I), we decompose the dipole moment of the *i*th ion, $\boldsymbol{p}_i$, into the permanent and induced terms, $\boldsymbol{p}_i = \boldsymbol{\mu}^{perm}_i + \boldsymbol{\mu}_i$, and accordingly represent χ^{WI} as follows

$$\chi^{WI} = \chi^{WI,perm} + \chi^{WI,ind} \tag{9a}$$

$$\chi^{WI,perm} = \frac{i\omega_{IR}}{2k_BT}\int_0^\infty e^{i\omega_{IR}t}\langle \sum_i^{wat}\sum_j^{ion} \boldsymbol{\alpha}_i(t)\boldsymbol{\mu}^{perm}_j(0)\rangle \tag{9b}$$

$$\chi^{WI,ind} = \frac{i\omega_{IR}}{2k_BT}\int_0^\infty e^{i\omega_{IR}t}\langle \sum_i^{wat}\sum_j^{ion} \boldsymbol{\alpha}_i(t)\boldsymbol{\mu}_j(0)\rangle \tag{9c}$$

Figure 6 also displays the $\chi^{WI,ind}_{iiz}$ component with the dotted black lines. By comparing $\chi^{WI,ind}_{iiz}$ with χ^{WI}_{iiz} (red lines), we can clearly see that $\chi^{WI,ind}_{iiz}$ has little contribution to χ^{WI}_{iiz} in the 3000−3600 cm^{-1} region, indicating that $\chi^{R,WI}_{iiz}$ is dominated by the $\chi^{WI,perm}_{iiz}$ term. The vibrational component $\boldsymbol{\mu}^{perm}_i$ of ions in the $\chi^{WI,perm}_{iiz}$ term is obviously attributed to the intramolecular vibration of hydronium cations since the dipole of the halide anions has no vibrational component in this frequency range, except for that of the induced electronic polarization.

To help assign the vibrational mode of the hydronium ions, Figure 7 displays the vibrational density of state, $I^{vdos}(\omega)$, for the hydronium ions at the surface layer with the black line, and the computational procedure of the spectral density is described in the Appendix. The total spectral density I^{vdos} consists of two bands, at about 3300 and 3400 cm^{-1}. The decomposition in

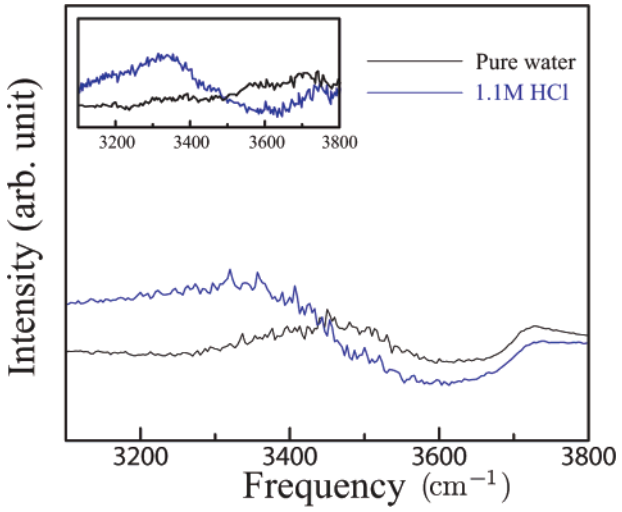

Figure 9. Calculated SFG spectra of sps polarization, I_{sps}^{SFG}, for a 1.1 M HCl solution (blue) and pure water (black). The inset shows the experimental SFG spectra of a 0.8 M HCl solution and pure water by Tarbuck et al.[30]

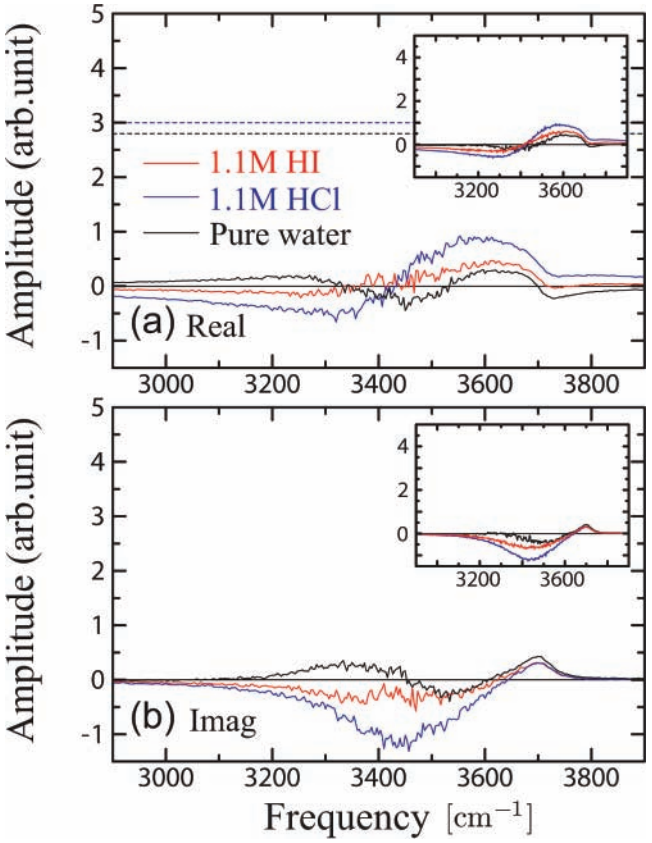

Figure 10. (a) Real and (b) imaginary parts of the *izi* ($i = x, y$) nonlinear susceptibility, χ_{izi}^{R}, for HCl and HI solutions and pure water. The insets show the self-part, χ_{izi}^{R}(self). The dashed horizontal lines in panel a indicate the level of $-\chi_{izi}^{NR}$.

Figure 7 clearly characterizes that the former band is assigned to the symmetric OH stretching of hydronium ions, while the latter is assigned to the degenerate OH stretching. This assignment supports that the vibration of hydronium ions contributing to $\chi_{iiz}^{R,WI}$ at about 3300 cm^{-1} is mainly from their symmetric OH stretching mode. The importance of the symmetric stretching mode is intuitively understood by considering the typical orientation of surface hydronium ions, with their dipole antiparallel to the surface normal ($\langle\cos\theta\rangle \approx -1$ in Figure 3).

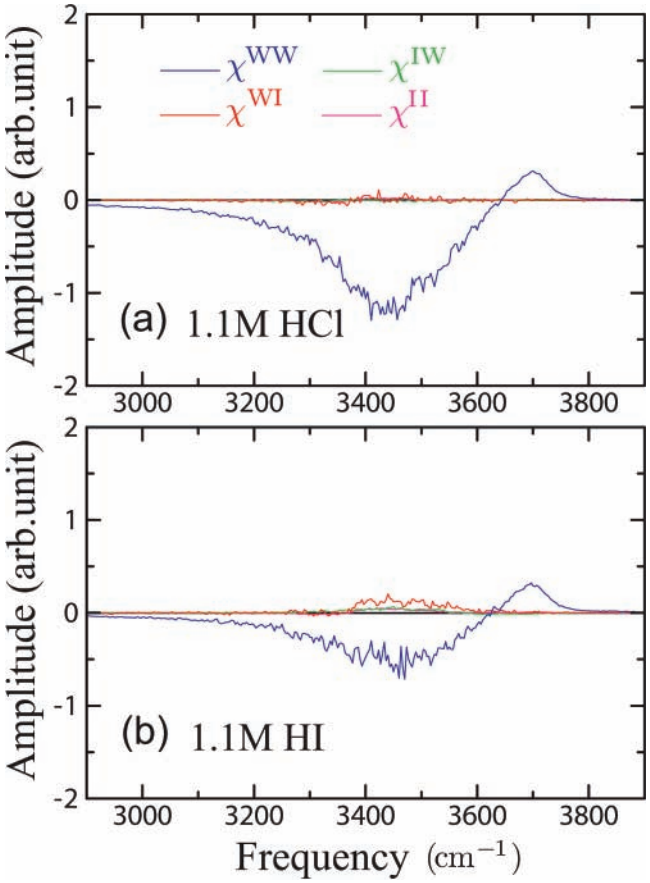

Figure 11. Decomposed amplitudes of Im[χ_{izi}^{R}] from eq 7 for HCl (panel a) and HI (panel b) solutions.

According to the selection rule, therefore, the symmetric OH stretching mode of the surface hydronium ions has a transition dipole parallel to the *z* direction, while the degenerate OH stretching modes are parallel to the interface. Consequently, the degenerate stretching modes should be much less active than the symmetric stretching mode in $\chi_{iiz}^{R,WI}$.[29]

The water−hydronium coupling mechanism in $\chi_{iiz}^{R,WI}$ is illustrated in Figure 8, assuming strong correlation in a typical local hydrogen-bonding complex, where a surface hydronium ion donates a hydrogen bond to a neighboring water molecule in the next monolayer. As schematically illustrated in Figure 8, the transition dipole of the symmetric stretching mode of a hydronium ion along the surface normal (red arrow) can couple to the transition dipole of water (blue arrow) either in phase or out of phase. It is conceivable that the in-phase coupling causes a red shift of the vibrational frequency and also brings a negative contribution to Im[$\chi_{iiz}^{R,WI}$], whereas the out-of-phase coupling causes vice versa. In the in-phase situation (left panel of Figure 8), for example, the transition dipole of water in the negative *z* direction (blue arrow) is correlated to increased polarizability α_{ii} of water. Thus, the change in sign of Im[$\chi_{iiz}^{R,WI}$] in Figure 6 is qualitatively elucidated by the above water−ion coupling mechanism.

4.2. The sps-Polarized Spectra. Figure 9 shows the calculated sps-polarized SFG spectra of a 1.1 M HCl solution and pure water, where the vibrationally resonant susceptibility χ_{izi}^{R} is calculated as a function of the infrared frequency in section 2.2 and the nonresonant term χ_{izi}^{NR} is empirically determined with a real constant value so as to best describe the experimental spectra. The experimental spectra reported by Tarbuck et al.[30] are shown in the inset for comparison. We note that the

experimental spectrum for the HI solution has not yet been reported, and therefore, the value of χ_{izi}^{NR} is not available at present, though χ_{izi}^{R} has been computed also for the HI case. In the case of the HCl solution, the calculated and the experimental sps spectra consistently show a broad band centered at about 3350 cm^{-1} and a broad dip at about 3600 cm^{-1}. Though this spectral line shape of the HCl solution is apparently different from that of the NaCl or NaI solution,[23] we argue that these features are consistently understood in terms of the different direction of the electric double-layer structure for these solution surfaces as follows.

Nonlinear Susceptibility χ_{izi}^{R}. The vibrationally resonant susceptibility χ_{izi}^{R}, calculated by eq 4, is displayed in Figure 10 for the HCl and HI solutions and pure water. We note that the line shape of χ_{izi}^{R} for the HI solution is calculated to exhibit an intermediate behavior between those for pure water and the HCl solution. In the case of the HCl solution, a large negative band is dominant in $\mathrm{Im}[\chi_{izi}^{R}]$ (panel b) at about 3400 cm^{-1}, and the sign of $\mathrm{Re}[\chi_{izi}^{R}]$ (panel a) changes accordingly there from negative to positive like a Lorentzian shape. We see that this large band of $\mathrm{Im}[\chi_{izi}^{R}]$ and the associated low-frequency negative tail of $\mathrm{Re}[\chi_{izi}^{R}]$ construct the broad band in the sps spectrum (Figure 9) at a frequency lower than ~3400 cm^{-1}. On the other hand, the positive part of $\mathrm{Re}[\chi_{izi}^{R}]$ at about 3600 cm^{-1} causes the dip of the sps SFG spectrum for the HCl solution (Figure 9) as a consequence of interference with the nonresonant background χ_{izi}^{NR}.

Figure 10 also shows the self-part, $\chi_{izi}^{R}(\mathrm{self})$, calculated by eq 6b in the insets. In a comparison of $\chi_{izi}^{R}(\mathrm{self})$ with χ_{izi}^{R}, the contribution of $\chi_{izi}^{R}(\mathrm{corr})$ for the HCl solution is found to be less significant in a quantitative sense than the for the sodium halide solutions.[23] Qualitative explanation for that difference is not obvious, though it implies that the correlation effect is not constructive at the HCl solution surface. This issue should be further pursued in the future. In the followings, we characterize the large band centered at about 3400 cm^{-1} using the decomposition analysis for the species in section 2.3.

Figure 11 shows the decomposed amplitudes of $\mathrm{Im}[\chi_{izi}^{R}]$ from eq 7 into $\mathrm{Im}[\chi_{izi}^{R,WW}] + \mathrm{Im}[\chi_{izi}^{R,WI}] + \mathrm{Im}[\chi_{izi}^{R,IW}] + \mathrm{Im}[\chi_{izi}^{R,II}]$ for the HCl (panel a) and HI (panel b) solutions. It can be easily seen that the water−water correlation term, $\chi_{izi}^{R,WW}$, dominates the total χ_{izi}^{R}, and the other three components, $\chi_{izi}^{R,WI}$, $\chi_{izi}^{R,IW}$, and $\chi_{izi}^{R,II}$ are much less significant for either solution. The negligible contribution of $\chi_{izi}^{R,IW}$ or $\chi_{izi}^{R,II}$ is readily understood in the same way as in the ssp cases discussed in section 4.1; the ion polarizability has a little vibrational component in the OH stretching frequency region. The reason for the small amplitude for $\chi_{izi}^{R,WI}$ is less obvious, though it should be attributed to the lack of orientational correlation between the hydronium ion and water in the tangential direction to the interface. We presume that this issue is related to the small contribution of $\chi_{izi}^{R}(\mathrm{corr})$ discussed above, though the clearer explanation for these issues needs to be presented through further analysis.

Water Orientation Reflected in χ_{izi}^{R}. Finally, we discuss the sign and amplitude of $\chi_{izi}^{R,WW}$ in relation to the orientational structure of water. As discussed in our previous study on salt (NaCl and NaI) solutions,[23] the sign of $\mathrm{Im}[\chi_{izi}^{R,WW}]$ reflects the direction of the OH bonds of water molecules. In the salt solutions, $\mathrm{Im}[\chi_{izi}^{R,WW}] > 0$ at about 3400 cm^{-1} is elucidated from the orientation of surface water and $\langle \cos\theta \rangle > 0$, indicating that the water molecules tend to direct their dipoles toward the vapor phase due to the electric double-layer formation.[22]

In the present case of acid solutions, both the signs of $\mathrm{Im}[\chi_{izi}^{R,WW}]$ and $\langle \cos\theta \rangle$ are reversed. $\mathrm{Im}[\chi_{izi}^{R,WW}] < 0$ at about 3400 cm^{-1} in Figure 11 is fully consistent with the orientation of surface water, and $\langle \cos\theta \rangle < 0$ is shown in Figure 2, which means that the water molecules tend to direct their dipoles toward the liquid phase. Furthermore, a more negative $\langle \cos\theta \rangle$ for HCl than that for HI in Figure 2 accounts for the larger negative amplitude of $\mathrm{Im}[\chi_{izi}^{R,WW}]$ for the HCl solution (panel a of Figure 11) than that for the HI solution (panel b). The difference in the sign of $\mathrm{Im}[\chi_{izi}^{R,WW}]$ at about 3400 cm^{-1} for the acid and salt solutions, which manifests a remarkable difference in the sps SFG line shapes, is indicative of the reversed electric field by the ionic double-layer formation.

5. Concluding Remarks

The molecular dynamics simulation of aqueous HCl and HI solution surfaces was applied to compute and analyze the recently reported experimental ssp- and sps-polarized SFG spectra. The calculation elucidated a number of experimental features of the SFG spectra, through investigating their surface structure and the nonlinear susceptibility. The present MD simulation supports that the hydronium ions are enriched at the topmost layer, consistent with other previous studies, and thereby the electric double-layer formation by the hydronium ions at the topmost surface and the halide anions slightly beneath. Thus, the direction of the ionic double layer for the acid solutions tends to be reversed from that of salt (NaCl, NaI) solutions, which has a significant impact on the water structure and manifests in the observed SFG spectra. In the case of the ssp spectra, the remarkably enhanced SFG intensity at about 3200 cm^{-1} is attributed to the two mechanisms, the ordered orientation of surface water due to the ionic double layer and the symmetric OH stretching mode of the surface hydronium ions. Apparent differences in the sps spectra of the acid and salt solutions are elucidated from the reversed sign of χ_{izi}^{R} at about 3200 cm^{-1}, which is indicative of the local water orientation oppositely perturbed by the ions.

Finally, we make some comments on the remaining issues. First, the surface potential of the acid solutions remains still unsolved, as pointed out by Randles[24] and mentioned in section 1. Molecular-level explanation of the surface potential is needed to reconcile this observation with the local surface structure predicted by the MD simulation. Second, the present Article mainly deals with the local structure of water, while the molecular model of the hydronium ion should be further examined, particularly when its spectral quantities are treated at ~3000 cm^{-1} or lower. This issue is related to the quantum effects of protons, though the strong preference for the surface is shown to be insensitive to the details of the model.[26]

Acknowledgment. This work was supported by the Next Generation Super Computing Project, Nanoscience Program, MEXT, Japan.

Appendix: Vibrational Density of State at the Interface

To aid in assigning vibrational spectra, the vibrational density of state is computed and decomposed into vibrational modes. The decomposition is utilized particularly to investigate the contribution of hydronium cations in the O−H stretching region in section 4. This appendix focuses on the spectral density calculation for hydronium.

The vibrational density of state is given as the Fourier transformation of the mass-weighted velocity autocorrelation function of the sites

$$I^{\mathrm{vdos}}(\omega) = \int_0^\infty \mathrm{d}t \cos(\omega t) \sum_i^{\mathrm{mol}} \sum_k^{\mathrm{site}} \sum_\alpha^{x,y,z} m^{k,i} \langle \dot{x}_\alpha^{k,i}(t) \dot{x}_\alpha^{k,i}(0) \rangle \quad (10)$$

$$= \int_0^\infty \mathrm{d}t \cos(\omega t) \sum_i \sum_k \sum_\alpha \frac{1}{m^{k,i}} \langle p_\alpha^{k,i}(t) p_\alpha^{k,i}(0) \rangle \quad (11)$$

where $m^{k,i}$ is the mass of the kth site of ith molecule and $\dot{x}_\alpha^{k,i}(t)$ and $p_\alpha^{k,i}(t) = m^{k,i}\dot{x}_\alpha^{k,i}(t)$ are the velocity and momentum of the site at time t for the α direction of the Cartesian coordinate. In eq 10 or 11, contribution of each molecule i is apparently additive. Therefore, one can straightforwardly calculate the spectral density for the hydronium ions by restricting the summation over i to the hydronium.

The spectral density I^{vdos} is represented using a set of internal vibrational coordinates $\{q_m^i\}$ of the ith hydronium ion as

$$I^{\mathrm{vdos}}(\omega) = \sum_{m,n} I_{mn}^{\mathrm{vdos}}(\omega) \quad (12)$$

$$I_{mn}^{\mathrm{vdos}}(\omega) = \int_0^\infty \mathrm{d}t \cos(\omega t) \sum_{i,k,\alpha} \frac{1}{m^{k,i}} \left\langle P_m^i(t) \frac{\partial q_m^i(t)}{\partial x_\alpha^{k,i}(t)} P_n^i(0) \frac{\partial q_n^i(0)}{\partial x_\alpha^{k,i}(0)} \right\rangle \quad (13)$$

where P_m^i is the conjugate momentum of q_m^i and $\partial q_m/\partial x_\alpha^k$ is usually called the B matrix in the vibrational analysis. For the OH stretching vibration of the hydronium ion, the internal coordinates are given as

$$\begin{cases} q_1^i = (r_1^i + r_2^i + r_3^i)/\sqrt{3} \\ q_2^i = (2r_1^i - r_2^i - r_3^i)/\sqrt{6} \\ q_3^i = (r_2^i - r_3^i)/\sqrt{2} \end{cases} \quad (14)$$

where $\{r_j^i\}$ ($j = 1, 2, 3$) denotes three OH bond lengths of the ith hydronium ion. Consequently, q_1^i and (q_2^i, q_3^i) correspond to the symmetric OH stretching mode and the degenerate OH stretching modes, respectively, of the ith ion.

In the calculation of Figure 7, the summation over i is restricted to the hydronium ions for the vapor side from $\hat{z} = -4.24$ Å, where the density minimum is located in Figure 1a. Thereby, the hydronium ions at the surface layer are selectively sampled. The calculated I^{vdos} in Figure 7 is decomposed into $I_{1,1}^{\mathrm{vdos}}$ and $I_{2,2}^{\mathrm{vdos}} + I_{3,3}^{\mathrm{vdos}}$. We confirmed that other components of $I_{m,n}^{\mathrm{vdos}}(\omega)$, including cross terms ($m \neq n$), are negligible compared to the three diagonal terms in the frequency range of Figure 7.

References and Notes

(1) Jungwirth, P.; Tobias, D. J. *Chem. Rev.* **2006**, *106*, 1259.
(2) Gopalakrishnan, S.; Liu, D.; Allen, H. C.; Kuo, M.; Shultz, M. J. *Chem. Rev.* **2006**, *106*, 1155.
(3) Onsager, L.; Samaras, N. N. T. *J. Chem. Phys.* **1934**, *2*, 528.
(4) Knipping, E. M.; Lakin, M. J.; Foster, K. L.; Jungwirth, P.; Tobias, D. J.; Gerber, R. B.; Dabdub, D.; Finlayson-Pitts, B. J. *Science* **2000**, *288*, 301.
(5) Garrett, B. C. *Science* **2004**, *303*, 1146.
(6) Shen, Y. R. *Principle of Nonlinear Optics;* Wiley: New York, 1984.
(7) Boyd, R. W. *Nonlinear Optics;* Academic Press: San Diego, CA, 2003.
(8) Eisenthal, K. B. *Chem. Rev.* **1996**, *96*, 1343.
(9) Miranda, P. B.; Shen, Y. R. *J. Phys. Chem. B* **1999**, *103*, 3292.
(10) Richmond, G. L. *Chem. Rev.* **2002**, *102*, 2693.
(11) Buck, M.; Himmelhaus, M. *J. Vac. Sci. Technol., A* **2001**, *19*, 2717.
(12) Vidal, F.; Tadjeddine, A. *Rep. Prog. Phys.* **2005**, *68*, 1095.
(13) Wang, H.; Gan, W.; Lu, R.; Rao, Y. B. W. *Int. Rev. Phys. Chem.* **2005**, *24*, 191.
(14) Shultz, M. J.; Schnitzer, C.; Simonelli, D.; Baldelli, S. *Int. Rev. Phys. Chem.* **2000**, *19*, 123.
(15) Shen, Y. R.; Ostroverkhov, V. *Chem. Rev.* **2006**, *106*, 1140.
(16) Morita, A.; Hynes, J. T. *Chem. Phys.* **2000**, *258*, 371.
(17) Morita, A.; Hynes, J. T. *J. Phys. Chem. B* **2002**, *106*, 673.
(18) Morita, A. *J. Phys. Chem. B* **2006**, *110*, 3158.
(19) Perry, A.; Neipert, C.; Space, B.; Moore, P. B. *Chem. Rev.* **2006**, *106*, 1234.
(20) Walker, D. S.; Hore, D. K.; Richmond, G. L. *J. Phys. Chem. B* **2006**, *110*, 20451.
(21) Ishiyama, T.; Morita, A. *Chem. Phys. Lett.* **2006**, *431*, 78.
(22) Ishiyama, T.; Morita, A. *J. Phys. Chem. C* **2007**, *111*, 721.
(23) Ishiyama, T.; Morita, A. *J. Phys. Chem. C* **2007**, *111*, 738.
(24) Randles, J. E. B. *Phys. Chem. Liq.* **1977**, *7*, 107.
(25) Dang, L. X. *J. Chem. Phys.* **2003**, *119*, 6351.
(26) Mucha, M.; Frigato, T.; Levering, L. M.; Allen, H. C.; Tobias, D. J.; Dang, L. X.; Jungwirth, P. *J. Phys. Chem. B* **2005**, *109*, 7617.
(27) Petersen, M. K.; Iyenger, S. S.; Day, T. J. F.; Voth, G. A. *J. Phys. Chem. B* **2004**, *108*, 14804.
(28) Shin, J. W.; Hammer, N. I.; Diken, E. G.; Johnson, M. A.; Walters, R. S.; Jaeger, T. D.; Duncan, M. A.; Christie, R. A.; Jordan, K. D. *Science* **2004**, *304*, 1137.
(29) Baldelli, S.; Schnitzer, C.; Shultz, M. J. *Chem. Phys. Lett.* **1999**, *302*, 157.
(30) Tarbuck, T. L.; Ota, S. T.; Richmond, G. L. *J. Am. Chem. Soc.* **2006**, *128*, 14519.
(31) Schnitzer, C.; Baldelli, S.; Shultz, M. J. *J. Phys. Chem. B* **2000**, *104*, 585.
(32) Radüge, C.; Pflumio, V.; Shen, Y. R. *Chem. Phys. Lett.* **1997**, *274*, 140.
(33) Levering, L. M.; Sierra-Hernández, M. R.; Allen, H. C. *J. Phys. Chem. C* **2007**, *111*, 8814.
(34) Jungwirth, P.; Tobias, D. J. *J. Phys. Chem. B* **2002**, *106*, 6361.
(35) Markovich, G.; Perera, L.; Berkowitz, M. L.; Cheshnovsky, O. *J. Chem. Phys.* **1996**, *105*, 2675.
(36) Sagnella, D. E.; Tuckerman, M. E. *J. Chem. Phys* **1998**, *108*, 2073.
(37) Brancato, G.; Tuckerman, M. E. *J. Chem. Phys.* **2005**, *122*, 224507.
(38) Wei, X.; Shen, Y. R. *Phys. Rev. Lett.* **2001**, *86*, 4799.
(39) Petersen, P. B.; Saykally, R. J. *J. Phys. Chem. B* **2005**, *109*, 7976.
(40) Du, Q.; Superfine, R.; Freysz, E.; Shen, Y. R. *Phys. Rev. Lett.* **1993**, *70*, 2313.
(41) Ostroverkhov, V.; Waychunas, G. A.; Shen, Y. R. *Phys. Rev. Lett.* **2005**, *94*, 046102.